Celestial Mech Dyn Astr (2006) 96:99–127
DOI 10.1007/s10569-006-9034-9

ORIGINAL ARTICLE

The Non-Gravitational Perturbations impact on the BepiColombo Radio Science Experiment and the key rôle of the ISA accelerometer: direct solar radiation and albedo effects

David M. Lucchesi · Valerio Iafolla

Received: 17 May 2005 / Revised: 7 March 2006 /
Accepted: 29 May 2006 / Published online: 10 October 2006

Abstract The paper is focused on the estimate of the impact of the non-gravitational perturbations on the orbit of the Mercury Planetary Orbiter (MPO), one of the two spacecrafts that will be placed in orbit around the innermost planet of the solar system by the BepiColombo space mission. The key rôle of the Italian Spring Accelerometer (ISA), that has been selected by the European Space Agency (ESA) to fly on-board the MPO, is outlined. In the first part of the paper, through a numerical simulation and analysis we have estimated, over a time span of several years, the long-period behaviours of the disturbing accelerations produced by the incoming direct solar radiation pressure, and the indirect effects produced by Mercury's albedo. The variations in the orbital parameters of the spacecraft, together with their spectral contents, have been estimated over the analysed period. The direct solar radiation pressure represents the strongest non-gravitational perturbation on the MPO in the very complex radiation environment of Mercury. The order-of-magnitude of this acceleration is quite high, about 10^{-6} m/s^2, because of the proximity to the Sun and the large area-to-mass ratio of the spacecraft. In the second part of the paper, we concentrated upon the short-period effects of direct solar radiation pressure and Mercury's albedo. In particular, the disturbing accelerations have been compared with the ISA measurement error and the advantages of an on-board accelerometer are highlighted with respect to the best modelling of the non-gravitational perturbations in the strong radiation environment of Mercury. The readings from ISA, with an intrinsic noise level of about 10^{-9} m/s$^2/\sqrt{\text{Hz}}$ in the frequency band of $3\cdot10^{-5}$–10^{-1} Hz, guarantees a very significant

D. M. Lucchesi (✉)· V. Iafolla
Istituto di Fisica dello Spazio Interplanetario, IFSI/INAF, Via Fosso del Cavaliere n. 100,
00133 Roma, Italy
e-mail: david.lucchesi@ifsi-roma.inaf.it

D. M. Lucchesi
Istituto di Scienza e Tecnologie della Informazione, ISTI/CNR, Via Moruzzi n. 1,
56124 Pisa, Italy
e-mail: David.Lucchesi@isti.cnr.it

reduction of the non-gravitational accelerations impact on the space mission accuracy, especially of the dominant direct solar radiation pressure.

Keywords Non-gravitational perturbations · Artificial satellites · Accelerometers · Mercury · Gravimetry · General relativity

1 Introduction

The European Space Agency (ESA) BepiColombo Cornerstone mission to Mercury consists of two spacecrafts to be placed in orbit around the innermost member of our planetary system (Grard and Balogh 2001; Spohn et al. 2001). One is the Mercury Magnetospheric Orbiter (MMO), characterised by a set of instruments for the study of Mercury's magnetic field, waves and particles in the environment of the planet as well as in the solar wind. The other is the Mercury Planetary Orbiter (MPO), characterised by a set of instruments in order to study Mercury's surface topography and composition, as well as the planet gravity field and rotational state. The present paper is related to the MPO spacecraft and the Radio Science Experiment (RSE), one of the main experiments considered for BepiColombo.

The MPO spacecraft will be nadir pointing and 3-axis stabilised. Its polar orbit will be characterised by a relatively high eccentricity of about 0.162 and a semimajor axis of about 3389 km[1], corresponding to a 2.32-h orbital period around Mercury. In order to perform the RSE it is necessary to allocate on-board the MPO a set of dedicated instruments. These instruments allow the determination of the MPO orbit around the planet and the accurate determination of Mercury's center-of-mass orbit around the Sun, by which it is possible to estimate several parameters related to the planet structure and verify the theory of general relativity (GR) (Milani et al. 2001, 2002; Iess and Boscagli 2001). The scientific goals to achieve by very precise measurements are: (i) the rotational state of Mercury; (ii) the global gravity field of Mercury and its temporal variations due to solar tides; (iii) the local gravity anomalies; (iv) the orbit of Mercury's center-of-mass around the Sun and the propagation of electromagnetic waves between the Earth and the spacecraft. In this way we will be able to constrain (i) the size and physical state of the core of the planet; (ii) the internal structure of the planet; (iii) the mantle structure of the planet and the interface between mantle and crust, respectively; and to improve (iv) the determination of the parameterized post-newtonian (PPN) parameters of GR.

These kinds of measurements are based on: (a) range and range-rate derivations of the MPO position with respect to Earth-bound radar station(s) by means of a High Gain Antenna (HGA); (b) the determination of the non-gravitational signals on the MPO by means of an on-board accelerometer; (c) the determination of the MPO absolute attitude by means of a Star-Tracker; (d) the determination of angular displacements of reference points on the solid surface of the planet by means of a High Resolution Camera (HRC). The range and range-rate derivations of the MPO position and velocity are based on the same technique applied to the CASSINI spacecraft (Bertotti et al. 2003a). A full 5-way link (Iess and Boscagli 2001) to the MPO (Ka-band and X-band channels with a mix mode with both) will provide an accuracy of about 10^{-12} for range and a few parts in 10^{-10} for range-rate. Indeed, by exploiting the frequency dependence of the refraction index, information on the plasma along

[1] With a perigee height of 400 km and an apogee height of 1500 km.

the path followed by the radio waves will be obtained, allowing for its calibration. This two-dimensional (range and range-rate) observation of Mercury's heliocentric motion is at a level of accuracy superior of the ground-based radar measurements.[2]

One of the instruments involved in the RSE is a very high sensitivity accelerometer able to measure the inertial accelerations acting on the MPO, i.e., it allows the deduction of the perturbing non-gravitational accelerations. The Italian Spring Accelerometer (ISA) has been considered and then selected by ESA to fly on-board the MPO (Iafolla and Nozzoli 2001). The non-gravitational perturbations (NGP) are critical for the RSE, especially the disturbing effects produced on the MPO orbit by the incoming visible solar radiation pressure. Indeed, the radiation environment around Mercury is quite strong. For instance, in the case of the visible radiation effects, the solar irradiance varies between 14,448 W/m^2 at Mercury's perihelion, to 6,272 W/m^2 at Mercury's aphelion (i.e., with a variation of about 80% at half of the sidereal period of Mercury around the Sun). For an Earth orbiting satellite, i.e., at one astronomical unit, the average value of the solar irradiance is just 1,366.1 W/m^2 with a minimum–maximum variation of just 0.37%. Moreover, the NGP are proportional to the *area-to-mass* ratio of the orbiting spacecraft, and this explains why Earth satellites, like the LAGEOS (LAser GEOdynamics Satellite), are characterised by a very low value of their *area-to-mass* ratio in order to minimise the NGP disturbing effects (Cohen and Smith 1985).

The present work is focused on the estimate of the impact of the long-period effects of the NGP on the MPO polar orbit, and over the characteristic time span (short-period effects) that will be typically used, in the gravimetry and general relativity experiments, for the recovery of the MPO orbit in the RSE. We study, through a numerical simulation and analysis, the disturbing effects on the MPO orbit due to the direct solar radiation pressure and Mercury's albedo radiation pressure. The effects due to Mercury's infrared radiation will be analysed in a forthcoming paper. We stress that the modelling of the NGP is not requested for the BepiColombo mission to Mercury because of the presence of the ISA accelerometer.

Our purpose is to prove the superiority of the readings from an on-board accelerometer with respect to the modelling of the NGP. Moreover, since we are interested in the estimate of the disturbing effects of the various NGP on the MPO orbit and, in particular, to their comparison with the readings from an on-board accelerometer, we assume – for the sake of simplicity – the MPO spherical in shape with an *area-to-mass* ratio of the planned spacecraft of $1.9 \cdot 10^{-2}$ m^2/kg, corresponding to a mass of approximately 357 kg.[3] In Tables 1 and 2, the MPO orbital parameters and Mercury dynamical-and-physical properties that have been used in the numerical simulation performed in this work are shown. The paper is organised as follows. In Sect. 2, we briefly introduce the accelerometer characteristics and performances. In Sects. 3 and 4, we describe the long-period effects due to the direct solar radiation pressure and to Mercury's albedo radiation. In Sect. 5, these disturbing NGP are analysed over a 7-h period and compared with the accelerometer measurement error. Finally, in Sect. 6 the conclusions and future work are outlined.

[2] Because of the higher frequencies and plasma compensation and because the equivalent radar-bounce-point will be the planet's center-of-mass.

[3] As we shall see in the following sections, the details of the evolution of the MPO orbit due to the true shape of the spacecraft are negligible at this level because of the superiority of the accelerometer readings.

Table 1 The MPO orbital parameters

Orbital parameter	Symbol	Numerical value
Semimajor axis	a	3389 km
Eccentricity	e	0.162
Inclination	I	90°
Orbital period	P	8355 s
Ascending node longitude	Ω	0°
Argument of perigee	ω	0.7°

The values used for the spacecraft initial ascending node longitude and initial argument of perigee are indicative only. Their "true" values will depend on the final orbit configuration of the MPO around Mercury

Table 2 Mercury's dynamical and physical properties

Orbital parameter	Symbol	Numerical value
Semimajor axis	a_{m}	$57.91 \cdot 10^6$ km
Eccentricity	e_{m}	0.206
Inclination	I_{m}	7.005°
Orbital (sidereal) period	P_{m}	87.969 days
Obliquity	ϵ_{m}	$\approx$0.1°
Mass	M_{m}	$3.30 \cdot 10^{23}$ kg
Radius	R_{m}	$\simeq$2439 km
Normal. coeff. ($\ell = 2, m = 0$)	C_{20}	$-(2.7 \pm 0.9) \cdot 10^{-5}$
Normal. coeff. ($\ell = 2, m = 2$)	C_{22}	$(1.6 \pm 0.8) \cdot 10^{-5}$

The values of the normalised harmonic coefficients C_{20} and C_{22} of Mercury's gravity field are from Anderson et al. (1987) while the other quantities may be found in Bertotti et al. (2003b)

2 The Italian Spring Accelerometer (ISA)

In the following we briefly highlight some of the accelerometer features that will be useful for the subsequent sections, in particular for the precise orbit determination (POD) process that will characterise the RSE. We focus on the following aspects: (i) ISA measurement principle and ISA performances in relation with the arc length during the POD analysis; (ii) ISA thermal control; (iii) ISA inflight calibration.

2.1 Measurement principle and performances

ISA is a three-axis torsional oscillator with an intrinsic noise of 10^{-9} m/s$^2/\sqrt{\mathrm{Hz}}$ in the frequency band of $3 \cdot 10^{-5}$–10^{-1} Hz. Each mechanical oscillator is obtained by manufacturing a single piece of aluminum (Al 5056) with the proof-mass connected to an external rigid frame by a crank-shaped suspension and with its sensitive axis orthogonal to the proof-mass flat face, see Fig. 1. The sensitive elements work like three independent (torsional) harmonic oscillators characterised by a very low resonance frequency of 3.5 Hz. The displacements of the proof-masses from their equilibrium positions are detected by means of capacitive transducers in a bridge configuration, followed by low noise amplifiers (Iafolla and Nozzoli 2001), see Fig. 2.

As described in Milani et al. (2001), the typical arc length for the POD process will be about $7 \div 8$ h,[4] while, in order to reach the ambitious goals of the RSE, it

[4] Between 4 h and 12 h depending on the spacecraft visibility conditions.

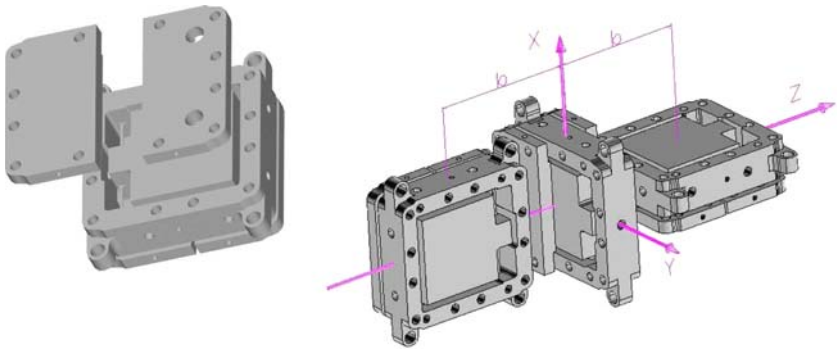

Fig. 1 One mechanical sensitive unit of the three-axis Italian Spring Accelerometer (left) and its geometrical configuration inside the MPO spacecraft (right). The three center-of-mass of the three proof-masses of the accelerometer are aligned along the MPO rotation axis (Z-axis) with ISA center-of-mass (that of the central proof-mass) coincident with the spacecraft (nominal) center-of-mass (COM). The sensitive axis of the central proof-mass is aligned with the MPO rotation axis (along the out-of-plane direction), while the sensitive axis of the other proof-masses (5 cm above or below the accelerometer center-of-mass) are aligned, respectively, along the radial and transversal directions

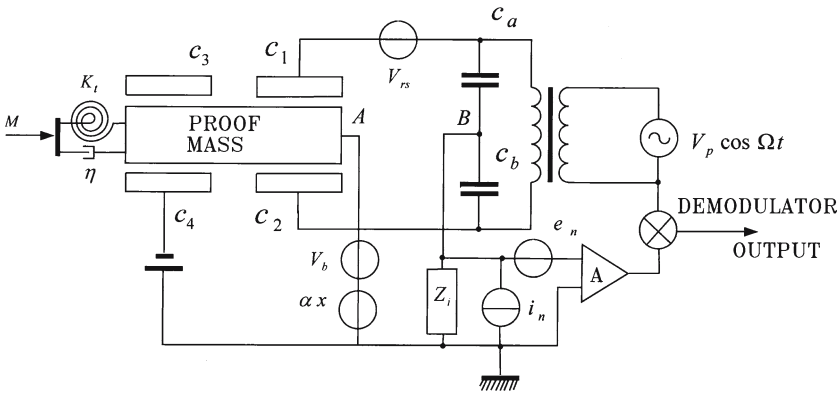

Fig. 2 ISA measurement principle. The detection of the disturbing acceleration is provided by a capacitor transducer in a bridge-like configuration followed by a very low noise amplifier. The bridge is biased at a frequency $f_p = 10$ kHz much higher than the oscillator resonance frequency $f_0 = 3.5$ Hz. The disturbing accelerations on the proof-mass cause the bridge unbalance and a modulation of the bias voltage. At the output of the capacitive bridge the signal is measured at the two sidebands $f_\pm = f_p \pm f_s$, where f_s represents the frequency of the disturbing acceleration. In this way, because the amplifier works at high frequency, we are able to avoid its $1/f$ noise

is necessary an accuracy in the along-track orbit reconstruction of about 1 m over 1 orbital revolution of the MPO around Mercury, i.e., over 8355 s. Therefore, the accelerometer bandwidth has been extended to lower frequencies ($3 \cdot 10^{-5}$ Hz) with respect to the original value (10^{-4} Hz) given in Iafolla and Nozzoli (2001), see Iafolla et al. (2006).

With regard to the along-track orbit reconstruction, the requested accuracy corresponds to an along-track acceleration accuracy of about 10^{-8} m/s^2. Therefore, this number has been considered equivalent to the accelerometer measurement error over the typical arc length during one observation session from the Earth's ground antenna(s), i.e., over the POD process.

2.2 Active thermal control

The impact of thermal effects on the accelerometer measurements, if not properly accounted for, may cause systematic errors in the results of Mercury's gravity field coefficents determination as well as in the estimate of the relativistic parameters (Milani et al. 2001, 2002). In fact, an accelerometer behaves also like a thermometer, which transforms a temperature variation in an equivalent acceleration. The experimental value of ISA thermal stability is about $5 \cdot 10^{-7}$ m/s^2/°C, that is 1°C of variation of the proof-mass temperature produces an equivalent acceleration of about $5 \cdot 10^{-7}$ m/s^2 along its sensitive axis.

The thermal effects appear both on long time scales, as at the revolution period of Mercury (about 88 days) and at half of this period, and on shorter time scales, as at the MPO orbital period (8,355 s). The former are at very low frequency, outside the accelerometer bandwidth, and will produce, again if not properly accounted for, a bias and a slope in the accelerometer readings during the orbit fit (i.e., over each arc observing session). The latter are inside the accelerometer bandwidth and will superimpose and mix with other periodic disturbing effects as well as with the non-gravitational accelerations.

The temperature variations (peak-to-peak) estimated for the mentioned thermal effects are about 25°C in the case of the long-period effects, and about 4°C in the case of the effects at MPO orbital period (ESA document SCI-PB/RS/1140 2004).

Therefore, in order to avoid these effects, an active thermal control (Iafolla et al. 2006) will be used to attenuate their impact on the accelerometer readings.[5]. The results of the experimental activity performed in our laboratory has presently produced an attenuation factor of about 700, both at the Mercury revolution period and at the MPO orbital period. This attenuation is more than sufficient in order to reach the goals of the RSE. Indeed, from the simulations of the gravimetry and relativity experiments it has been proved that it is enough an attenuation of a factor 100 of the long-period thermal effects in order to guarantee the ambitious objectives of the RSE.

2.3 Inflight calibration

The inflight calibration of an accelerometer represents a quite thorny issue. Usually, the expression *inflight calibration* refers to the estimate, as unknowns during the POD fit, for a bias and a scale factor in order to correct the accelerometer readings and consequently transform them in absolute measurements. However, this very important aspect represents only a piece of the complex set of procedures necessary to calibrate an accelerometer, once in orbit. In our case, by inflight calibration of ISA accelerometer we mean the following main aspects:

1. to verify, using ISA actuators, that ISA response to a known acceleration is the same that was obtained on-ground;
2. to verify, using the accelerometer control capacitors, that ISA transfer function is still flat below the accelerometer resonance frequency;
3. the knowledge of the position of each center-of-mass (*com*) of the accelerometer proof-masses with respect to the MPO center-of-mass (*COM*), and of the

[5] Moreover, three thermometers will be used to measure the temperature behaviour for each proof-mass of the accelerometer during the space mission life.

orientation of each proof-mass sensitive axis with respect to the MPO frame (principal axes of inertia);
4. estimate of ISA scale factor and bias for each arc during the POD analysis of the RSE.

Point 1 is related with the knowledge of ISA transducer factor and its possible variation with respect to the on-ground value after the in-orbit injection. Point 2 implies that we are confident to have the desired measurement error inside ISA bandwidth. Point 3 is related with the occurence of possible masses movements and distortions inside the spacecraft during the launch of the BepiColombo mission and/or the final injection of the spacecraft into its polar orbit around Mercury.

In order to perform the calibrations described at point 3 we can spin the MPO spacecraft along its principal axes of inertia with a known profile for the angular rate and for the angular acceleration along each axis[6] and measure the corresponding accelerations on the three proof-masses of the accelerometer. Then, from a least square fit we can calibrate the accelerometer response and extract the relative displacements between the accelerometer proof-masses *com* with respect to the spacecraft *COM*, as well as the accelerometer sensitive axes alignment with respect to the MPO frame.

Let us now describe a little more point 4 above. During each arc of the POD that will characterise the RSE, in order to account for unmodelled effects a bias and a scale factor are estimated together with other parameters that are necessary for the MPO orbit determination. These two unknowns are estimated for the radial, the transversal and the out-of-plane directions, respectively. The mathematical relation useful to approximate the accelerometer measurements (one for each sensitive axis) is:

$$A_{\mathrm{m}} \simeq S_f A_{\mathrm{t}} + B \tag{1}$$

where A_{m} and A_{t} are the measured acceleration and the true acceleration, respectively, while S_f and B are the proof-mass scale factor and bias. The estimate of the bias B for each arc is quite important. Indeed, the critical aspect is related with how the bias can change with time during the observing session.

It could be useful to have some apriori values of S_f and B by comparison of the accelerometer readings with some model for the NGP. Of course, we use an accelerometer because of its superiority with respect to the NGP models we can built for the MPO, anyway, at this level, some modelling may help us (in a sort of iterative procedure) to calibrate the accelerometer for the POD process. We emphasize that this calibration, arc-by-arc, of the accelerometer links intimately ISA with the RSE goals.

3 Direct solar radiation pressure

The resultant acceleration produced by the direct solar radiation pressure (SRP) on a spherical satellite is:

[6] This procedure can be accomplished using the spacecraft reaction wheels.

$$\vec{a}_{\odot} = -\frac{A\Phi_{\odot}}{mc}\left(\frac{\overline{R}_{\odot}}{R_{\odot}}\right)^2 \hat{S} \tag{2}$$

where A/m represents the *area-to-mass* ratio of the satellite, c the speed of light, $\Phi_{\odot}$ the solar irradiance at the average distance $\overline{R}_{\odot}$ of Mercury from the Sun, and $\hat{S}$ represents the unit vector towards the Sun. The squared term is due to the modulation coming from the large eccentricity of Mercury's orbit around the Sun. In Eq. 2 we neglect the diffusive term of the reflected radiation (i.e., we assumed one for the value of the spacecraft radiation coefficient), while the penumbra effects are being considered in our numerical simulations because of the vicinity of the Sun. In particular, the fraction of the total sunlight in the penumbra has been computed (see Baker 1967).

In the following, we focus on the long-period effects produced by the direct SRP perturbation. In particular, in Subsect. 3.1 we show the behavior of the components—in the Gauss form—of the disturbing acceleration over a 3-years period, while in Subsect. 3.2 the effects of the disturbing acceleration on the MPO orbit are described.

3.1 Long-period behavior of the solar radiation pressure components

As a consequence of the extreme variations of the solar irradiance over Mercury's orbit, the disturbing acceleration due to the direct solar radiation vary in the range between $4 \cdot 10^{-7}$ m/s^2 and $1 \cdot 10^{-6}$ m/s^2, i.e., it is much larger than the acceleration on the LAGEOS satellite,[7] the best tracked Earth-orbiting satellite through the powerful Satellite Laser Ranging technique. In order to analyse the orbital effects produced by the disturbing acceleration on the satellite (Subsect. 3.2) and because of the three-axis accelerometer, it is useful to decompose the SRP acceleration in three orthogonal components according to the Gauss form (Milani et al. 1987): (i) along the radial direction (from Mercury's center-of-mass to the MPO); (ii) along the out-of-plane direction (i.e., along the angular momentum direction); and (iii) transversely in the orbital plane (perpendicular to the other two directions).

The following long-period numerical simulation has been performed computing the three components of the disturbing acceleration each 15 days with a 1° step size along the spacecraft orbit around the planet. Of course, in order to retain the long-term effects, the three disturbing accelerations have been averaged over 1 orbital revolution of the MPO around Mercury in order to average out the short period effects.

In Fig. 3—over a 3-years time span[8]—the radial component of the solar radiation pressure and its spectral analysis are shown.[9] As we can see the main effect is at half of Mercury's sidereal period (i.e., at 44 days), with peak amplitudes of about $2.5 \cdot 10^{-7}$ m/s^2 in magnitude. Figure 4 shows the results of our numerical simulation for the transversal component of the disturbing acceleration and for its spectral analysis. As we can see, an oscillation with a period of about 88 days (i.e., close to the sidereal period of Mercury) is superimposed to a longer oscillation.[10] From this figure, it is clear that the oscillation with the 88-days period is superimposed to an oscillation

[7] About $3.6 \cdot 10^{-9}$ m/s^2, thanks also to its smaller *area-to-mass* ratio.

[8] The nominal mission duration expected for the MPO around Mercury is 1 year.

[9] The vertical axis represents the normalised coefficient of spectral correlation.

[10] In order to solve for this longer effect, we extended our numerical simulation to a period of 4,995 days (about 13.7 years).

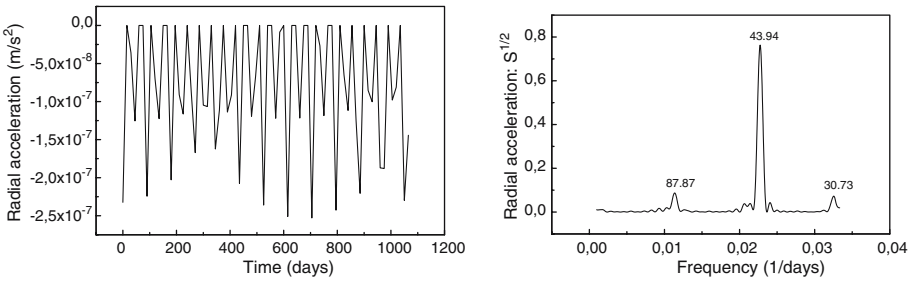

Fig. 3 Radial component (m/s^2) of the direct solar radiation pressure perturbation over a three years time span (left) and its spectral content (right). The main frequency is given by the $2\dot{\lambda}$ line, at half of the sidereal period of Mercury around the Sun. There is also a clear evidence of the $\dot{\lambda}$ frequency (at the sidereal period of Mercury, equal to 87.969 days) and of a line with a period of about 30.7 days

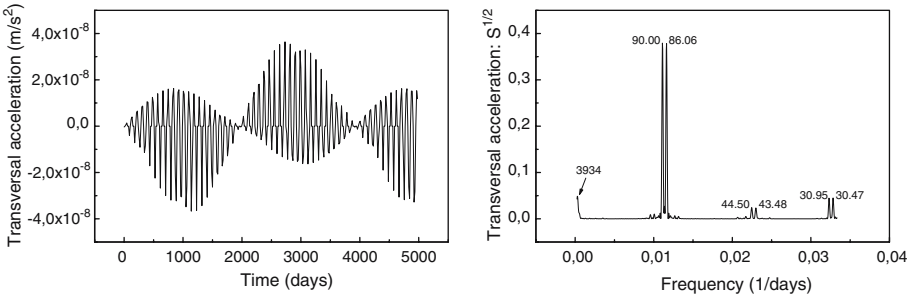

Fig. 4 Transversal component (m/s^2) of the direct solar radiation pressure perturbation over more than 13 years (left) and its spectral content (right). The two main lines are close to the periods of 89.99 days and 86.05 days, which corresponds to the spectral lines $\dot{\omega} - \dot{\lambda}$ and $\dot{\omega} + \dot{\lambda}$, i.e., the combination of Mercury's longitude around the Sun and of the MPO argument of perigee. On the left side of the spectrum, there is the evidence of the MPO argument of perigee spectral line, which is very clear in the time evolution of the acceleration. The other two couples of lines close to the 44-days period and to the 30-days period are given by the spectral lines $\dot{\omega} \pm 2\dot{\lambda}$ and $\dot{\omega} \pm 3\dot{\lambda}$, respectively, see Table 3 in the text

characterised by a period close to 4000 days. This long periodicity is related with the argument of perigee rate of the MPO as discussed below. The transversal component of the acceleration reaches peaks close to $3.5 \cdot 10^{-8}$ m/s^2, with periodicities which are a combination of Mercury's sidereal longitude, λ, and of the MPO argument of perigee, ω. Figure 5 refers to the out-of-plane component of the direct SRP acceleration. The larger effects are in the case of the out-of-plane component of the disturbing acceleration, with peak amplitudes close to $8 \cdot 10^{-7}$ m/s^2 and a well defined periodicity at the sidereal period of Mercury around the Sun.

With regard to the spectral content of the three components of the disturbing acceleration, the results obtained can be easily interpreted taking the scalar product of Eq. 2 with the three unit vectors along the Gauss comoving frame.[11] For instance, in the case of the transversal component we obtain:[12]

$$< T >_{2\pi} \simeq -e a_{\odot} \sin\omega \cos(\Omega - \lambda) \left(1 + 2e_{\mathrm{m}} \cos\lambda + \frac{1}{2} e_{\mathrm{m}}^2 + \frac{5}{2} e_{\mathrm{m}}^2 \cos 2\lambda\right) \qquad (3)$$

[11] See Sect. 3.2 and Eqs. 10, 11, 12 and 13.

[12] Here $<>_{2\pi}$ represents the average over one orbital revolution of the MPO around Mercury.

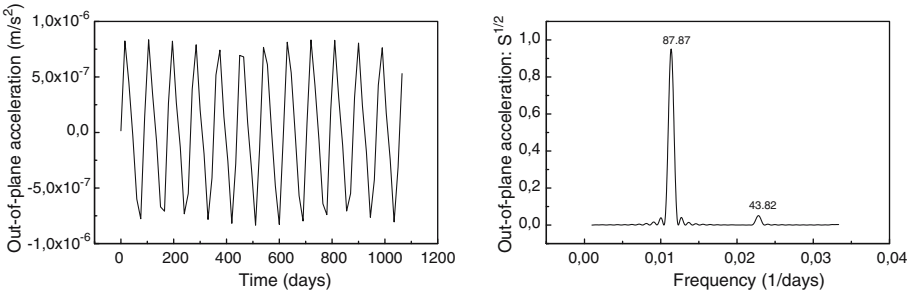

Fig. 5 Out-of-plane component (m/s^2) of the direct solar radiation pressure perturbation over a three years time span (left) and its spectral content (right). The spectral line related with Mercury's longitude rate $\dot{\lambda}$ is clearly visible and corresponds to Mercury's sidereal period around the Sun. Much smaller is the contribution from the $2\dot{\lambda}$ spectral line

where e_{m} represents Mercury's eccentricity. Therefore, as previously underlined, the spectral lines are given by the combination of the MPO argument of perigee ω and of Mercury's longitude λ around the Sun. In Table 3, the main lines with their periods are shown. These lines, in particular the strongest ones, are well reproduced in the spectrum of Fig. 4. Of course, we have not any contribution from the $\dot{\Omega}$ line because $\dot{\Omega} = 0$ for the MPO orbit. The amplitude of the lines $\dot{\omega} - \dot{\lambda}$ and $\dot{\omega} + \dot{\lambda}$ is larger with respect to the other lines because it is simply demultiplied by the satellite eccentricity (i.e., $ea_{\odot}$), while in the other cases it depends from the product of the MPO eccentricity e times Mercury's eccentricity e_{m}.

Rigorously, we have to notice that Eq. 2 is valid only in the absence of eclipses. In general, in the analytic approach, when we are interested to the correct frequency dependency we must multiple Eq. 2 times the eclipses function (see for instance, Ferraz Mello 1971, for the shadow function in the case of Earth's satellites). The effect is to introduce new spectral lines, mainly characterised by the combination of the planet longitude and the satellite ascending node longitude, as the line $2(\dot{\Omega} - \dot{\lambda})$ which governs the periodicity of the eclipses (see for instance, Lucchesi 2001, in the case of LAGEOS satellites). The eclipses effects are more effective in influencing the radial component of the direct SRP than the transversal one. Indeed, in the case of the radial component the main line is $2\dot{\lambda}$ with a 44-days period, which corresponds to the periodicity of the eclipses, while there is no clear evidence of the contribution coming

Table 3 Spectral lines of the transveral component T of the direct solar radiation pressure perturbation as determined through Eq. 3

Spectral line	Period
$\dot{\omega} + \dot{\lambda}$	86.05 days
$\dot{\omega} - \dot{\lambda}$	−89.99 days
$\dot{\omega} + 2\dot{\lambda}$	43.50 days
$\dot{\omega} - 2\dot{\lambda}$	−44.49 days
$\dot{\omega} + 3\dot{\lambda}$	29.11 days
$\dot{\omega} - 3\dot{\lambda}$	−29.55 days
$\dot{\omega}$	3934.05 days

from the $\dot{\omega}$ line.[13] In the case of the out-of-plane component we obtain:

$$< N >_{2\pi} \simeq - a_{\odot} \sin(\Omega - \lambda) \left(1 + 2e_{\mathrm{m}} \cos\lambda + \frac{1}{2}e_{\mathrm{m}}^2 + \frac{5}{2}e_{\mathrm{m}}^2 \cos 2\lambda\right) \tag{4}$$

The independency from the satellite eccentricity e explains why the out-of-plane components is the largest acceleration in the previous figures. The main spectral lines are $\dot{\lambda}$ (88-days period), $2\dot{\lambda}$ (44-days period) and $3\dot{\lambda}$ (29.3-days period). Their respective amplitude is proportional to $a_{\odot}$, $e_{\mathrm{m}}a_{\odot}$ and $e_{\mathrm{m}}^2 a_{\odot}$.

The results already obtained suggest that the main disturbing thermal signals on the MPO and, consequently, on the ISA accelerometer structure, are at the sidereal period of Mercury (≈88 days) and at half of the sidereal period (≈44 days),[14] respectively, due to the out-of-plane acceleration and to the radial one. The transversal component of the acceleration is responsible for a thermal effect close to the sidereal period of Mercury, due to the lines $\dot{\omega} \pm \dot{\lambda}$. However, for these periodicities, the amplitudes of the transversal component of the disturbing acceleration are smaller than those at the sidereal period (for the out-of-plane component) and half of the sidereal period of Mercury (for the radial component). This is very important because the transversal acceleration is the most significant component for the success of the gravimetry and general relativity experiments and, ultimately, for all the RSE goals.

3.2 The solar radiation pressure impact on the MPO orbit

In the following we focus on the orbital effects produced by the disturbing direct SRP acceleration. In particular, the results on the MPO semimajor axis, eccentricity, inclination, node and argument of perigee will be analysed. The Gauss perturbing equations have been used for the determination of the spacecraft osculating orbital elements rates (see Milani et al. 1987):

$$\frac{\mathrm{d}a}{\mathrm{d}t} = \frac{2}{n\sqrt{1-e^2}} \left[T + e(T\cos f + R\sin f)\right] \tag{5}$$

$$\frac{\mathrm{d}e}{\mathrm{d}t} = \frac{\sqrt{1-e^2}}{na} \left[R\sin f + T(\cos f + \cos u)\right] \tag{6}$$

$$\frac{\mathrm{d}I}{\mathrm{d}t} = \frac{N}{H} r\cos(\omega + f) \tag{7}$$

$$\frac{\mathrm{d}\Omega}{\mathrm{d}t} = \frac{N}{H\sin I} r\sin(\omega + f) \tag{8}$$

$$\frac{\mathrm{d}\omega}{\mathrm{d}t} = \frac{\sqrt{1-e^2}}{nae} \left[-R\cos f + T(\sin f + \frac{1}{\sqrt{1-e^2}}\sin u)\right] - \frac{\mathrm{d}\Omega}{\mathrm{d}t}\cos I \tag{9}$$

[13] In the non-eclipses case the result for $< R >_{2\pi}$ is equal to that of Eq. 3 with the term $\cos\omega$ instead of $-\sin\omega$.

[14] These results agree with the independent thermal analyses performed by the industrial contractors of ESA.

where H represents the orbital angular momentum per reduced mass of the two-body problem, while R, T and N are the components of the acceleration in the Gauss form along the radial, transversal and out-of-plane directions, respectively. In these equations the quantities a, e, I, Ω and ω are the satellite's semimajor axis, eccentricity, inclination, longitude of the ascending node and argument of perigee, respectively.[15] The fast angular variables f and u are the satellite's true anomaly and eccentric anomaly, finally n represents the satellite mean motion ($n = 2\pi/P$). The essence of the method is to write the time derivatives of the parameters characterising the perturbed satellite orbit, and then numerically integrate them in order to find the effects in the elements.

It is important to underline that in the following, in order to find the correct long-period behaviour of the orbital parameters of the MPO spacecraft, we need to perform our numerical simulation over a time span longer than that of the period of the satellite perigee rate. This is obvious in the case of the MPO semimajor axis rate (Eq. 5), because of the behaviour of the transversal component of the disturbing acceleration (see Fig. 4), but it is also true in the case of all the other orbital elements. It is actually easy to see that terms like $< R \sin f >_{2\pi}$, $< T \cos f >_{2\pi}$ in the previously introduced Gauss equations give a frequency dependence as that obtained in Eq. 3 for the transversal component of the acceleration.

We can introduce the unit vectors along the radial, $\hat{r}$, transversal, $\hat{t}$, and out-of-plane, $\hat{n}$, directions, as well as the Sun unit vector $\hat{S}$:

$$\hat{r} = \begin{Bmatrix} \cos\Omega\cos(\omega+f) - \sin\Omega\sin(\omega+f)\cos I \\ \sin\Omega\cos(\omega+f) + \cos\Omega\sin(\omega+f)\cos I \\ \sin(\omega+f)\sin I \end{Bmatrix} \tag{10}$$

$$\hat{t} = \begin{Bmatrix} -\cos\Omega\sin(\omega+f) - \sin\Omega\cos(\omega+f)\cos I \\ -\sin\Omega\sin(\omega+f) + \cos\Omega\cos(\omega+f)\cos I \\ \cos(\omega+f)\sin I \end{Bmatrix} \tag{11}$$

$$\hat{n} = \begin{Bmatrix} \sin\Omega\sin I \\ -\cos\Omega\sin I \\ \cos I \end{Bmatrix} \tag{12}$$

$$\hat{S} = \begin{Bmatrix} \cos\lambda \\ \sin\lambda\cos\epsilon_m \\ \sin\lambda\sin\epsilon_m \end{Bmatrix} \tag{13}$$

(where $\epsilon_{\mathrm{m}} \approx 0.1^\circ$ represents the obliquity of the Mercury orbit), then we can compute the three components R, T and N of the disturbing acceleration, introduce them into the Gauss equations and finally average over the spacecraft mean anomaly. For instance, in the case of the rate of the satellite ascending node longitude we obtain:

$$< \frac{\mathrm{d}\Omega}{\mathrm{d}t} >_{2\pi} = \frac{a_\odot}{H \sin I}\left(\frac{\overline{R}_\odot}{R_\odot}\right)^2 \sin(\Omega - \lambda) < r\sin(\omega+f) >_{2\pi} \tag{14}$$

[15] We will not discuss here with the perturbation on the spacecraft mean anomaly and the corresponding Gauss equation.

where $r = a(1 - e^2)/(1 + e\cos f)$ represents the satellite distance from Mercury's center-of-mass. Therefore, because $< \sin(\omega + f) >_{2\pi} = -e\sin\omega$ and $< e\sin(\omega + f)\cos f >_{2\pi} = (e/2)\sin\omega$, we finally obtain (considering only the frequency dependence):

$$< \frac{\mathrm{d}\Omega}{\mathrm{d}t} >_{2\pi} \propto \frac{3e}{2}\sin\omega\sin(\Omega - \lambda)\left(1 + 2e_m\cos\lambda + \frac{1}{2}e_{\mathrm{m}}^2 + \frac{5}{2}e_{\mathrm{m}}^2\cos 2\lambda\right) \qquad (15)$$

Hence, also the MPO nodal rate (and equivalently its inclination rate) which is proportional to the out-of-plane component N of the acceleration and not to the transversal one, is subjected to long-period effects which are characterised by a very long-period oscillation (with the argument of perigee periodicity, about 3934 days) with superimposed a shorter oscillation with the period of the sidereal motion of Mercury around the Sun (about 88 days).

3.2.1 Semimajor axis effects

Through our numerical simulation we have determined the effects produced by the SRP perturbation on the MPO semimajor axis rate (Eq. 5). The larger oscillations reach a peak amplitude of about 8 km/year in the rate, while the main spectral lines are the same as those found in the case of the transversal component of the disturbing acceleration, i.e., they are given by the combination of Mercury's longitude around the Sun and of the MPO argument of perigee. This can be easily interpreted from Eq. 5, where the main contribution to the semimajor axis rate derives from the effects produced by the transversal component of the acceleration ($\dot{a} \approx 2T/n$), while the other $(\omega + f)$-modulated terms are demultiplied by the satellite eccentricity e.

In Fig. 6, the integrated disturbing effect on the MPO semimajor axis is shown. The variations with respect to the nominal value of 3389 km grows up to about 5 km after about 2000 days, then the semi-major axis decreases to its nominal value again in a time span of about 2000 days. In this time evolution, the influence of the MPO argument of perigee periodicity ($\simeq$3934 days) becomes clear.

3.2.2 Eccentricity effects

The impact of the disturbing acceleration produced by the SRP on the spacecraft eccentricity is shown in Fig. 7. The spectral analysis coincide with that obtained in the case of the satellite semimajor axis rate. The eccentricity grows up to about $8 \cdot 10^{-3}$ over half of the MPO argument of perigee periodicity, then it decrease again to its nominal value of 0.162.

3.2.3 Inclination effects

The larger effects in the inclination rate are characterised by an amplitude of about $4 \cdot 10^5$ mas/year.[16] The spectrum is characterised by the $\dot{\omega} \pm \dot{\lambda}$ lines and by the $\dot{\omega} \pm 2\dot{\lambda}$ lines. The strongest spectral line is given by the $\dot{\omega} + \dot{\lambda}$ combination, with a periodicity of about 43.98 days. In Fig. 8, the integrated effect on the inclination of the MPO spacecraft is shown. The larger effects reach a maximum amplitude of about $8 \cdot 10^{-3}$ degrees.

[16] 1 mas/year (milli-arc-second per year).

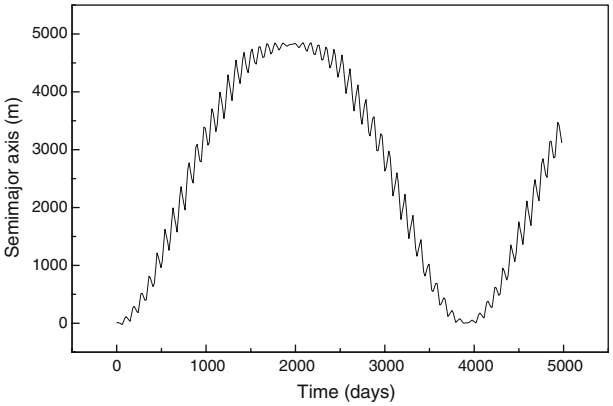

Fig. 6 Semimajor axis time evolution due to the direct solar radiation pressure perturbation over more than 13 years

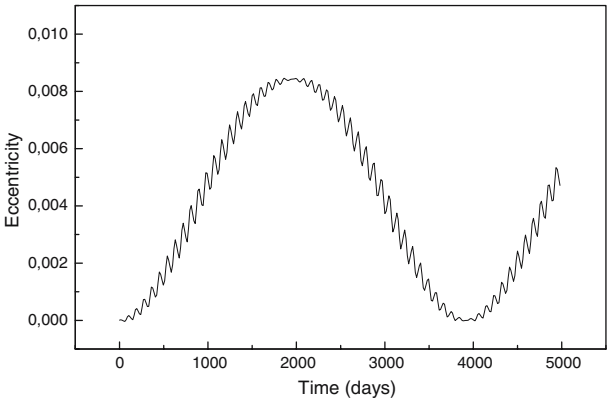

Fig. 7 Eccentricity time evolution due to the direct solar radiation pressure perturbation over more than 13 years

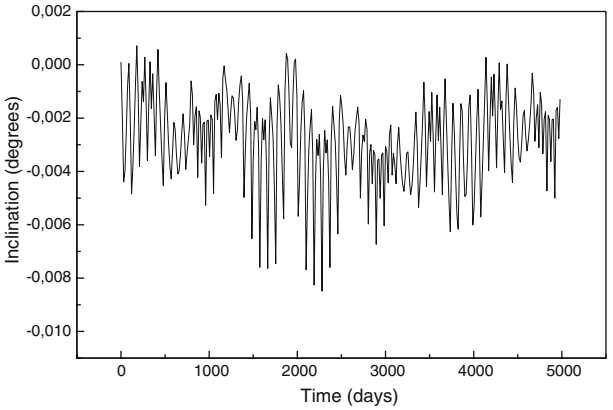

Fig. 8 Inclination time evolution due to the direct solar radiation pressure perturbation over more than 13 years

3.2.4 Node effects

The amplitude of the larger effects in the nodal rate is about $1.5 \cdot 10^5$ mas/year. The disturbing effects on the MPO node longitude due to the out-of-plane component of the direct SRP—as described by Eq. 8—are shown in Fig. 9. The impact on the node longitude is always smaller than $2.5 \cdot 10^{-3}$ degrees. The spectral analysis is characterised by the frequencies $\dot{\omega} - \dot{\lambda}$ and $\dot{\omega} + \dot{\lambda}$, respectively, at 89.93 days and 86.06 days.

3.2.5 Argument of perigee effects

The larger effects in the perigee rate are instead characterised by an amplitude of about $1.3 \cdot 10^7$ mas/year, about two orders-of-magnitude larger than inclination and node rates. The results of the numerical analysis of Eq. 9 have been integrated in order to obtain the effects on the spacecraft argument of perigee, see Fig. 10. Concerning the Fourier analysis the main spectral lines are dominated by the $\dot{\omega} - \dot{\lambda}$ and

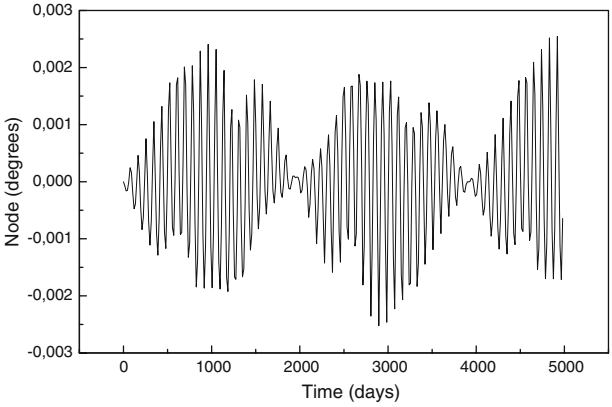

Fig. 9 Ascending node longitude time evolution due to the direct solar radiation pressure perturbation over more than 13 years

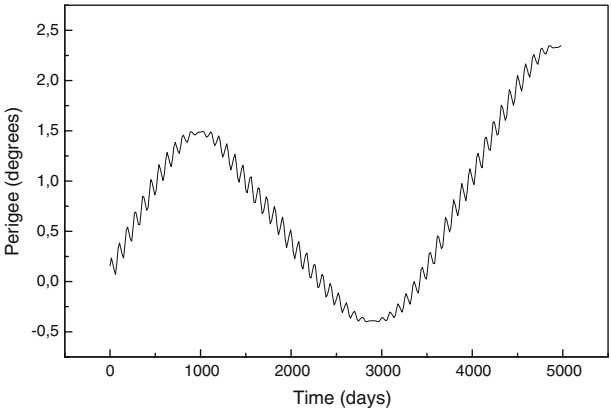

Fig. 10 Argument of perigee time evolution due to the direct solar radiation pressure perturbation over more than 13 years

$\dot{\omega} + \dot{\lambda}$ lines, but there is also a clear evidence of the argument of perigee spectral line, $\dot{\omega}$, with approximately a 3934-days period. The larger effects on the argument of perigee are reached after 1000 days, with a value of about 1.5° —which corresponds to an along-track displacement $a\omega$ of about 89 km—and after 5000 days, with a value of about 2.3° —which corresponds to an along-track displacement of about 136 km.

3.3 Discussion

The results obtained in the previous sections prove the strong impact of the perturbation produced by the direct solar radiation pressure on the orbital elements of the MPO spacecraft. It is interesting to compare these results on the MPO orbit with those on the orbit of the two laser-ranged and Earth-orbiting LAGEOS satellites. We have previously evidenced that the direct SRP acceleration on LAGEOS-type satellite is much smaller than that on the MPO; indeed in the case of the Mercury orbiter the acceleration is $\approx 100 \div 300$ times larger—depending on the position of Mercury along its orbit around the Sun—because of its larger area-to-mass ratio ($1.9 \cdot 10^{-2}\,\mathrm{m^2/kg}$) with respect to that of LAGEOS ($6.95 \cdot 10^{-4}\,\mathrm{m^2/kg}$) and the larger values for the solar irradiance. Therefore, we expect that the effects obtained on the MPO orbit are more than two orders-of-magnitude larger than those on the orbit of the two LAGEOS satellites.

This is well confirmed by the results shown in the literature concerning the direct solar radiation perturbation impact on the two LAGEOS satellites (see for instance, Barlier et al. 1986; Vokrouhlický et al. 1993; Lucchesi 2001). Anyway, we simulated the direct SRP effects on LAGEOS II orbit over a time span of more than 10 years (3849 days) and we directly verified that the perturbing effects of the solar radiation are more than two orders of magnitude smaller in the case of the laser-ranged satellite. For instance, in the case of the semi-major axis rate, the disturbing effects on LAGEOS II are about 500 times smaller than those on the MPO, while the effects on LAGEOS II eccentricity rate are about a factor 600 smaller than those on the MPO. Similar considerations are valid also for the other analysed elements. In Fig. 11, the effects on LAGEOS II semimajor axis are shown. As we can see, over a period of about 4000 days the integrated effect in the element is just 2 m, about three orders of magnitude smaller than in the case of the MPO semimajor axis, see Fig. 6.

The SRP effects on the MPO orbit are so strong that they are competitive with the gravitational perturbations in modifying the spacecraft orbit. The values of the gravitational monopole term[17] in the case of the MPO and of LAGEOS II are comparable, $\simeq 1.9\,\mathrm{m/s^2}$ and $\simeq 2.7\,\mathrm{m/s^2}$, respectively. This means that the ratio $(GM/a^2)/a_\odot$ is about two-orders-of-magnitude larger in the case of LAGEOS II.

If we now consider the perturbing acceleration due to the oblateness of the primary

$$a_{\mathrm{obl}} = 3\frac{GM}{r^2}\left(\frac{R_m}{r}\right)^2 C_{20} \tag{16}$$

we obtain a value of about $1 \cdot 10^{-3}\,\mathrm{m/s^2}$ for LAGEOS II and about $8 \cdot 10^{-5}\,\mathrm{m/s^2}$ for the MPO around Mercury (the Earth's normalised quadrupole coefficient C_{20} is $4.84 \cdot 10^{-4}$, about a factor 20 larger than that presently estimated for Mercury). This acceleration is responsible for the main disturbing gravitational effects on the

[17] The leading gravitational acceleration GM/r^2 that influence the satellite's motion.

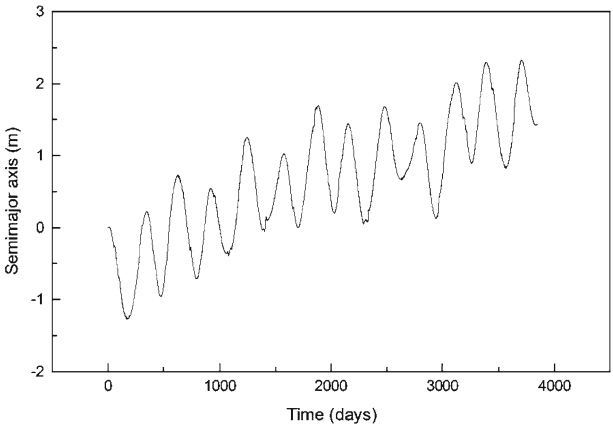

Fig. 11 LAGEOS II semimajor axis time evolution due to the direct solar radiation pressure perturbation over a 10-years time span

Keplerian elements of the unperturbed (two-body) orbit followed by a satellite. If we compare the values obtained for the perturbing gravitational acceleration with the corresponding perturbation due to the SRP, we obtain a ratio of about $3 \cdot 10^5$ for LAGEOS II and about 80 for the MPO. Therefore, the gravitational perturbation is much more effective for LAGEOS II than for the MPO around Mercury.

Indeed, if we compute explicitly the long-period effects of Mercury oblateness on the MPO orbital elements (which are characterised by the $2\dot{\omega}$ spectral line, see Kozai 1959), in particular on the spacecraft eccentricity and argument of perigee,[18] we obtain an impact on the elements much smaller than that previously obtained for the SRP, about a factor of 1000 smaller in amplitude.

This discussion highlights once more the importance of the measurement of the NGP by the accelerometer.

4 Mercury albedo radiation pressure

The "Bond albedo" of Mercury, i.e., the fraction of the incoming solar energy that is reflected into space, is generally low and has been estimated to be 0.119 (Vilas et al. 1988). Our knowledge of Mercury's surface reflectivities properties is incomplete and comes essentially from Mariner 10 flybys, through which only a fraction of the planet surface (about 45%) has been mapped into a photomosaic reconstruction. The local values of the albedo vary significantly over Mercury's surface, approximately between 0.09 and 0.45. The studies performed in order to estimate Mercury's albedo have produced the following results for the different typologies of the planet surface (see Smith and West 1983): (i) bright craters up to $\simeq$0.35; (ii) intercrater plains $\simeq$0.14; (iii) hummocky plains $\simeq$0.13; (iv) smooth plains $\simeq$0.12; (v) bright rays $\simeq$0.22; (vi) flat bottom craters $\simeq$0.15; (vii) secondary crater fields $\simeq$0.13. In our analysis a nominal

[18] There are no long-periodic terms in the semimajor axis, while there are no long-periodic effects in the inclination and ascending node longitude for a polar orbit.

albedo coefficient of 0.12 has been assumed with a *Lambertian* diffusion[19] from each surface element of Mercury.

The order-of-magnitude of the disturbing acceleration produced by the planet albedo on an orbiting spacecraft may be obtained through the following equation which simply rescales the effects of the direct SRP acceleration:

$$a_{\mathrm{alb}} = \frac{\overline{A}_{\mathrm{m}}}{2}\left(\frac{R_{\mathrm{m}}}{a}\right)^2 a_{\odot} \tag{17}$$

where $\overline{A}_{\mathrm{m}}$ and R_{m} are Mercury's average albedo ($\approx$0.12) and equatorial radius ($\simeq$2439 km), respectively. Therefore, the acceleration due to Mercury visible (albedo) radiation pressure (MVRP) is $\approx 1/30$ of that due to the direct SRP. In our numerical analysis, in order to determine the disturbing effects of MVRP on the MPO spacecraft we followed the approach developed by Rubincam and Weiss (1986) for the LAGEOS satellite (here $\ddot{\vec{a}}_{\mathrm{alb}}$ represents the albedo acceleration from each surface element of Mercury illuminated by the Sun and visible from the MPO spacecraft):

$$\ddot{\vec{a}}_{\mathrm{alb}} = a_{\odot}\rho^2\overline{A}_{\mathrm{m}}\cos\beta_{\mathrm{s}}\frac{(\cos\theta-\rho)}{\left(1-2\rho+\rho^2\right)^2}\left\{\begin{array}{l}[\sin\theta_{\mathrm{S}}\cos\theta_{\mathrm{S}}-\rho\sin\theta\cos\alpha]\,\hat{x}\\ +[\sin\theta_{\mathrm{S}}\sin\alpha_{\mathrm{S}}-\rho\sin\theta\sin\alpha]\,\hat{y}\\ +[\cos\theta_{\mathrm{S}}-\rho\cos\theta]\,\hat{z}\end{array}\right\}\frac{\mathrm{d}\Gamma}{\pi R_{\mathrm{m}}^2} \tag{18}$$

where $\rho = R_{\mathrm{m}}/a, \beta_{\mathrm{s}}$ represents the Sun zenith angle from the local vertical, (x, y, z) defines an equatorial reference frame, (θ, α) are the colatitude and longitude of the surface element $\mathrm{d}\Gamma$ with respect to Mercury's North pole, finally (θ_S, α_S) are the MPO coordinates with respect to the same origin.[20]

The integration problem is complicated because we must integrate twice the disturbing accelerations: (i) over the spherical cap seen by the satellite; and (ii) over one orbital revolution of the satellite in order to average out the short period effects. Therefore, we divided the Mercury visible cap seen by the satellite into concentric rings—centred in the sub-satellite point—with the same angular width $\delta\theta$, and each ring has been divided into a number of quasi-squared elements of constant area, i.e., with $\delta\alpha(\theta) = \delta\theta/\sin\theta$. Hence the area of each surface element $\mathrm{d}\Gamma$ is $\sin\theta\delta\theta\delta\alpha \simeq (\delta\theta)^2$. For the number of elements contained in the innermost (and smaller) cap around the sub-satellite point we obtained $\simeq\pi$. Thus, by putting three elements in the innermost cap and varying $\delta\theta$,[21] we obtain an almost uniform distribution of arbitrarily small, quasi-squared, surface elements (we refer to Lucchesi and Farinella 1992 for further details).

In the following, we focus on the long-period effects produced by MVRP perturbation: in Subsect. 4.1 we show the behavior of the components of the disturbing acceleration over 3 years, while in Subsect. 4.2 we describe the effects of the disturbing acceleration on the MPO orbit over 13.7 years.

[19] That is, for a given direction, the intensity of the diffused light is proportional to the cosine of the angle between the unit vector perpendicular to the surface element and the Sun direction.

[20] In Eq. 18 we used in our numerical integration the nominal albedo value 0.12 for each surface element $\mathrm{d}\Gamma$ of the spherical cap.

[21] In the numerical analysis we fixed $\delta\theta = 10°$ and we also assumed 10° for the integration step size over the MPO orbit.

4.1 Long-period behavior of the components of Mercury albedo acceleration

In Fig. 12, the radial component of MVRP and its spectral analysis are shown. As we can see the main effect is at half of Mercury's sidereal period (close to the 44 days periodicity), with peak amplitudes of about $1.4 \cdot 10^{-8}$ m/s^2 (and not smaller than $4 \cdot 10^{-9}$ m/s^2). Figure 13 shows the results of the numerical simulation in the case of the transversal component of the disturbing acceleration, while Fig. 14 refers to the

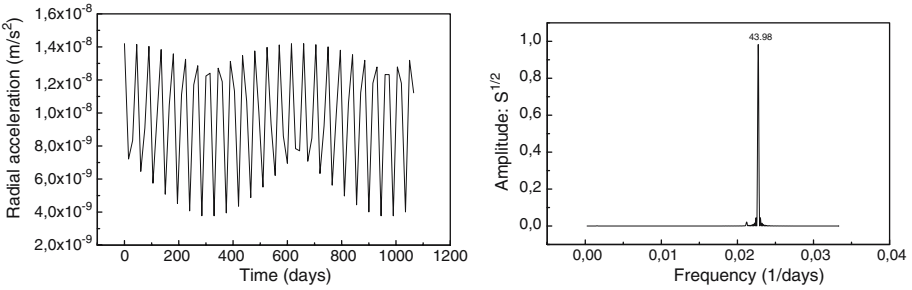

Fig. 12 Radial component (m/s^2) of Mercury albedo radiation pressure perturbation over a 3-years time span (left) and its spectral content (right). The main line is the $2\dot{\lambda}$ frequency, at half of the sidereal period of Mercury around the Sun, equal to 43.985 days

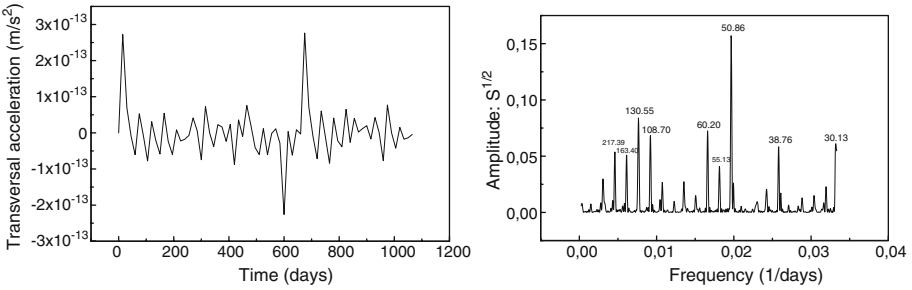

Fig. 13 Transversal component (m/s^2) of Mercury albedo radiation pressure perturbation over a 3-years time span (left) and its spectral content (right). The main line is close to the 50.86 days periodicity

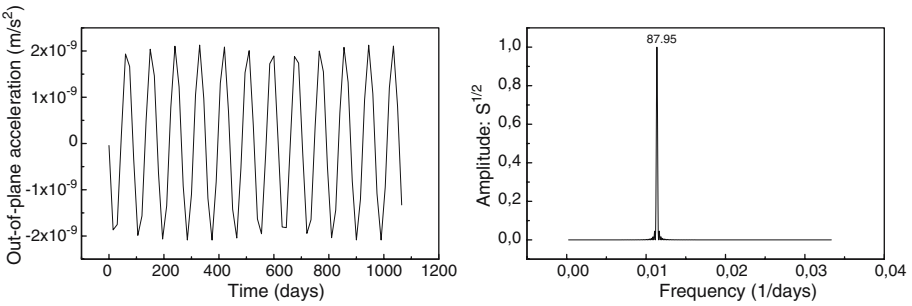

Fig. 14 Out-of-plane component (m/s^2) of Mercury radiation pressure perturbation over a 3-years time span (left) and its spectral content (right). The spectral line related with Mercury's longitude rate $\dot{\lambda}$ is clearly visible and corresponds to Mercury's sidereal period around the Sun

out-of-plane component of MVRP acceleration. The spectrum of the transversal component of the disturbing acceleration is quite rich, and we can recognise some of the lines shown in Table 3, but there is no clear evidence of the two main lines obtained in the case of the direct SRP perturbation, i.e., the $\dot{\omega} - \dot{\lambda}$ and $\dot{\omega} + \dot{\lambda}$ lines. The maximum amplitudes are close to $2.5 \cdot 10^{-13}$ m/s^2 in magnitude, i.e., they are much smaller than the contribution from the radial component of the disturbing acceleration. In the case of the out-of-plane component of the acceleration the maximum amplitudes are close to $2 \cdot 10^{-9}$ m/s^2, while the spectral analysis shows that the spectrum is dominated by the $\dot{\lambda}$ sidereal year line (close to the 88 days periodicity). Therefore, the disturbing components of Mercury's albedo acceleration are much smaller than those produced by the solar radiation. In particular, if the maximum values just obtained and those in Sect. 3 in the case of the direct SRP are compared, we obtain the order-of-magnitude ratio close to that computed with Eq. 17, i.e. MVRP = 1/30 SRP. As expected, the spectrum of the albedo radiation is quite similar to that of the solar radiation, with the main contribution from the lines at the sidereal period of Mercury (88 days) and at half of the sidereal period (44 days).

The larger effects are produced by the radial component of the albedo perturbation, with a maximum order-of-magnitude close to the accuracy ($\simeq 10^{-8}$ m/s^2) of the MPO orbit determination in the RSE via the Earth-tracking multiple frequency radiolink (Milani et al. 2001; Iess and Boscagli 2001). We describe deeply these aspects in Sect. 5.

4.2 Mercury albedo impact on the spacecraft orbit

From the results of the numerical analysis performed on the Gauss components of the albedo acceleration, it is clear that the disturbing effects on the MPO orbit produced by MVRP are much smaller than those previously obtained in the case of the direct SRP. Therefore, in the present section we will deal with the orbital effects on the MPO semimajor axis and argument of perigee only. Again, we numerically integrated Gauss equations over a 13.7-years time span.

4.2.1 Semimajor axis effects

We computed the disturbing effects of MVRP on the MPO semi-major axis rate and then the integrated effects on the orbit semimajor axis. The effects on the rate are more than two orders-of-magnitude smaller than those in the case of the direct SRP perturbation. The spectral analysis reveals, in addition to the main lines at $\dot{\omega} - \dot{\lambda}$ and $\dot{\omega} + \dot{\lambda}$ (with periods of 90.01 days and 86.06 days), two more lines at $\dot{\omega} - 2\dot{\lambda}$ and $\dot{\omega} + 2\dot{\lambda}$ (with periods of 44.48 days and 43.52 days). In Fig. 15 are shown the integrated effects on the spacecraft semimajor axis. The maximum variations with respect to the nominal value are close to 2 m, about three orders-of-magnitude smaller than those obtained in Fig. 6 in the case of the direct SRP perturbation.

4.2.2 Argument of perigee effects

In the case of the argument of perigee rate the largest amplitudes are about two orders-of-magnitude smaller than those obtained for the perturbation due to the SRP. The results of the spectral analysis agree—with concern to the main lines—with those obtained in the case of the direct SRP perturbation. However, as in the case

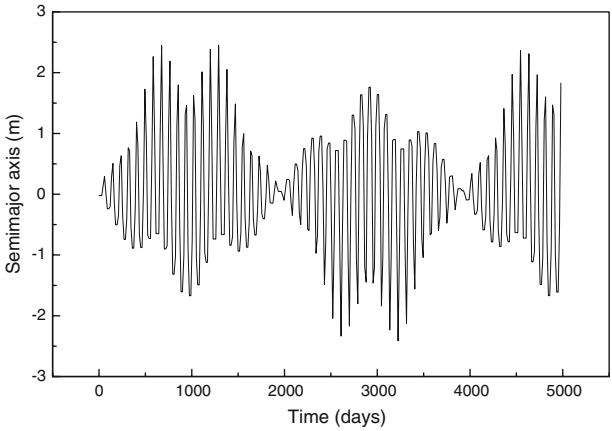

Fig. 15 Semimajor axis time evolution due to Mercury radiation pressure perturbation over more than 13 years

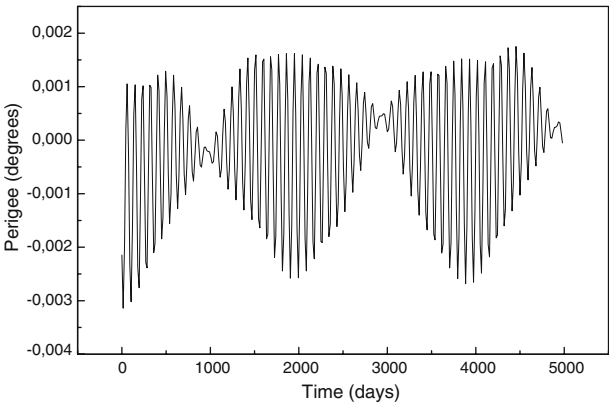

Fig. 16 Argument of perigee time evolution due to Mercury albedo radiation pressure perturbation over more than 13 years

of the semi-major axis rate, there is no evidence of the periodicity related with the satellite argument of perigee. Figure 16 shows the integrated effects on the spacecraft argument of perigee. As we can see, the effects on the perigee are more than two orders-of-magnitude smaller than those previously obtained in the case of the SRP perturbation, see Fig. 10.

5 Short period effects

It is well known from space geodetic techniques that it is not possible to determine the orbit of a spacecraft with an accuracy of the same level of the tracking data over a very long arc. It is necessary to decompose the long-arc in a number of shorter arcs, not causally connected, and solve for the initial conditions of the satellite state-vector (position and velocity) for each arc, together with a set of parameters in order to

absorb unmodelled or poorly modelled perturbations[22] (see for instance Milani et al. 1995; Tapley et al. 2004; Lucchesi and Balmino 2006).

Moreover, in the case of the complex set of experiments that characterise the RSE, the partitions into shorter arcs needs to consider the visibility conditions of the MPO from the Earth-bound radar station(s).[23] A full description of such problems is in Milani et al. (2001). The conclusion is that arcs not longer than a few hours must be considered (about 7–8 h on average) because the systematic long-period components in the accelerometer measurement errors result in several meters uncertainty of the satellite position after 1 day (see Sect. 2).

Therefore, in the following, we are interested to compare directly the effects due to the analysed NGP with the accelerometer measurement error over the typical arc length that will be used for the MPO orbit determination. In particular, it is also of importance to determine which signals are inside the accelerometer measurement bandwidth ($3 \cdot 10^{-5}$–10^{-1} Hz) and which are not. We assumed arc lengths equal to three orbital periods of the spacecraft around Mercury, i.e., approximately equal to 7 h. Again we distinguish between the solar effects (Sect. 5.1) and the albedo (Sect. 5.2) ones.

5.1 Short effects due to solar radiation pressure

Figure 17 shows the time evolution of the radial component of the SRP over three orbital periods of the MPO spacecraft around Mercury and its Fourier analysis, while in Fig. 18 the same is shown in the case of the transversal component of the disturbing acceleration. We omitted here to describe the out-of-plane component of the disturbing acceleration because, as described in Sect. 2, for the spacecraft orbit reconstruction we are mainly interested to the along-track component of the acceleration, and this component depends from the transversal and radial accelerations only. As we can see, the Fourier analyses reproduce correctly the (strongest) line at the spacecraft orbital period, i.e., the 8,355 s period, with the corresponding amplitude of about 10^{-6} m/s^2.

If we compare the results of Figs. 17 and 18 with the accuracy necessary for reaching the goals of the RSE, i.e., 10^{-8} m/s^2, we can see (especially in the case of the transversal component of the solar acceleration) that we are able to gain a factor 100—at the MPO orbital period—by taking into account the direct SRP perturbation with the use of the on-board accelerometer.[24] Moreover, besides the main effect at the spacecraft orbital period, there are other frequencies—still below 10^{-3} Hz—which are a factor 10 in magnitude above the 10^{-8} m/s^2 threshold. Therefore, the advantages of an on-board accelerometer, with the goal to account for the NGP of the spacecraft orbit, are evident.

Of course, we can also try to model the NGP and, in particular, the SRP perturbation. In this way one can argue that the advantages of the accelerometer are not so important. But this is not the case in reality. Indeed, the NGP are quite difficult to

[22] The two set of dynamical parameters we have described—that is those introduced to absorb poorly modelled effects and those corresponding to well understood effects which we are fitting—together with the satellite state-vector form the set of the so-called local parameters of the arc.

[23] The visibility conditions constrain the way in which range and range-rate measurements are collected. They can not be gained continuously, while the accelerometer measurements are available each 20 s.

[24] An accuracy of 10^{-8} m/s^2 in the acceleration measurement, against a maximum signal of about 10^{-6} m/s^2, implies a factor of 100 in the signal removal.

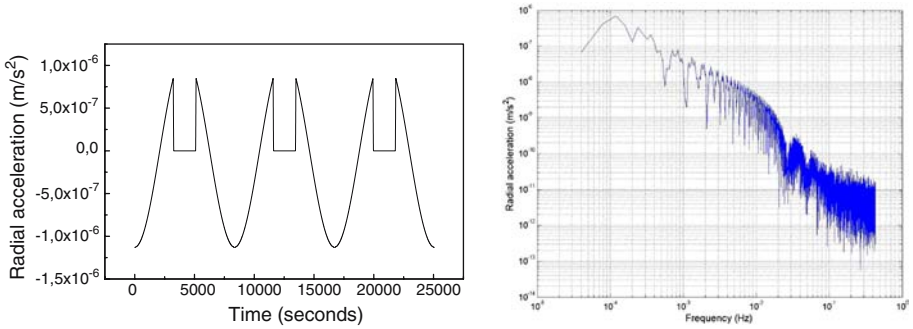

Fig. 17 Radial component of the solar radiation pressure over three orbital revolutions of the MPO around Mercury (left) and its Fourier analysis (right)

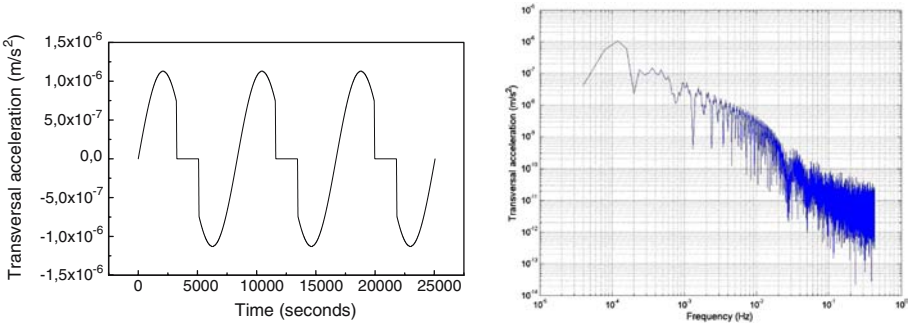

Fig. 18 Transversal component of the solar radiation pressure over three orbital revolutions of the MPO around Mercury (left) and its Fourier analysis (right)

model in the case of the MPO, even the simplest (but strongest) one, i.e., the direct solar radiation pressure. As we underlined in Sect. 1, the MPO will be very complex in shape, with solar panels, the High Gain Antenna (HGA) for tracking from Earth, thrusters for attitude-and-orbit manoeuvres, and on-board instrumentation. Therefore the spacecraft surface will reflect (in the visible) and reradiate (in the infrared) in a very complex way. All these aspects will limit our modelling accuracy to about 10% of the subtle and complex effects produced by the NGP (that is, a residual unmodelled perturbation, about 10^{-7} m/s^2 in magnitude, will be present in the POD process). Moreover, our knowledge of the optical properties of the various surfaces of the spacecraft will be limited by the strong radiation environment at work on the MPO. Indeed, these properties will degradate in time with unknown laws.[25] Therefore an accuracy of 10% of the NGP effect in modelling probably represents an optimistic view.

However, we stress that even in this case we are able to gain more than a factor 10 with the accelerometer. For instance, we are not able to correctly model the effects produced during the penumbra transitions before the spacecraft entering or exiting from the planet shadow. Instead, these subtle effects will be observed naturally by the accelerometer.

[25] For POD we need to know the optical properties of homogeneous surfaces.

It could be thought, in principle, to gain even more of the cited factor 10 with respect to the best modelling of the SRP by integrating over the measurement bandwidth of the ISA accelerometer. Indeed, the previous considerations have been based on an accuracy of the accelerometer (i.e., its measurement error over the chosen arc length) equal to $10^{-8}\,\mathrm{m/s^2}$, that is equal to the accuracy needed for the mission requirements. However, the ISA accelerometer intrinsic noise is about $10^{-9}\,\mathrm{m/s^2}/\sqrt{\mathrm{Hz}}$ in the frequency band $3 \cdot 10^{-5}$–$10^{-1}\,\mathrm{Hz}$. Therefore, assuming an accuracy of about $10^{-8}\,\mathrm{m/s^2}/\sqrt{\mathrm{Hz}}$ in the accelerometer measurement bandwidth[26] (in such a way to account for the environmental noise), it is enough an integration time of a few seconds to reach a $10^{-8}\,\mathrm{m/s^2}$ accuracy, while over three orbital periods of the MPO an accuracy of about $1.2 \cdot 10^{-10}\,\mathrm{m/s^2}$ can be reached. This will allow for more than two orders-of-magnitude gain with the use of the ISA accelerometer even in the case of the 10% modelling of the SRP perturbation.

Unfortunately, these arguments can be applied only to the random errors and not to the sinusoidal or pseudo-sinusoidal errors at the MPO orbital period. These pseudo-sinusoidal error sources are due to Mercury's gravity gradients and to the apparent forces on the rotating spacecraft. These errors are limited to a value of about $10^{-8}\,\mathrm{m/s^2}$ by the knowledge of the accelerometer position-and-error-matrix.[27]

Once the industrial contractor for building the MPO will be in charge, the final position-matrix for the accelerometer will be determined and maybe some margin is left for a possible integration over about 30–40 s. This would require smaller displacement-errors for the accelerometer position-matrix than those used in our conservative estimate for the accelerometer error budget. This will probably improve towards a factor of 30 gain with respect to the 10% modelling error. Anyway, such a gain is rigorously possible only if all the other sources of noise are constrained at the same level of the accelerometer measurement error.

5.2 Short effects due to Mercury albedo

In Figs. 19 and 20, we show the Fourier analyses of the radial and transversal components of the perturbation in the case of Mercury's albedo radiation, again over three orbital periods of the MPO. Of course, in this case, the peak accelerations are smaller ($\approx 10^{-8}\,\mathrm{m/s^2}$) than those obtained in the case of the SRP and comparable, in magnitude, with the accuracy requested by the RSE.

Therefore, the albedo effect can significantly be removed only if it is possible to operate with an accelerometer accuracy better than $10^{-8}\,\mathrm{m/s^2}$, as described previously in the case of the SRP.

6 Conclusions and future work

We have analysed the disturbing effects due to the incoming visible solar radiation pressure and Mercury's albedo on the MPO spacecraft, one of the two spacecrafts of the BepiColombo mission to Mercury. The spacecraft has been assumed spherical in shape but with the real area-to-mass ratio of the planned satellite. This simplification

[26] In reality, it is enough to assume such an accuracy only in the 10^{-4}–$10^{-3}\,\mathrm{Hz}$ interval of the measurement bandwidth. At higher frequencies the noise is dominated by the tracking error while, at lower frequencies, the thermal noise is dominant.

[27] That is, the matrix that gives the positions, in the spacecraft body frame, of the accelerometer proof-masses with their errors.

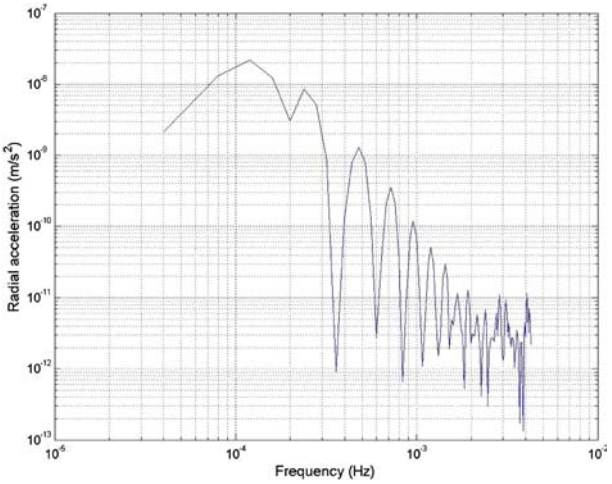

Fig. 19 Fourier analysis of the radial component of Mercury albedo radiation pressure over three orbital revolutions of the MPO around Mercury. At the orbital period the maximum acceleration is about $2 \cdot 10^{-8}$ m/s^2

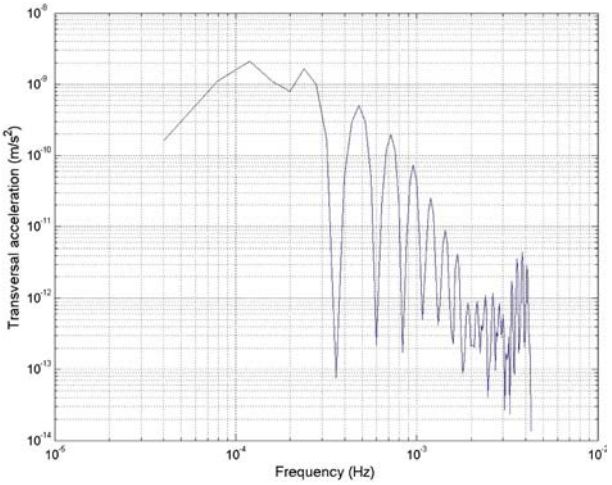

Fig. 20 Fourier analysis of the transversal component of Mercury radiation pressure over three orbital revolutions of the MPO around Mercury. At the orbital period the maximum acceleration is about $2 \cdot 10^{-9}$ m/s^2

of the complex shape of the spacecraft does not change the validity of our results because an on-board accelerometer has been considered to fly on the MPO and no modelling effort is therefore required for the disturbing NGP. The ISA accelerometer, developed at IFSI, will measure the NGP acting on the MPO. ISA is a three-axis room temperature accelerometer with an intrinsic noise of 10^{-9} m/s$^2/\sqrt{\text{Hz}}$ in the frequency band $3 \cdot 10^{-5}$–10^{-1} Hz.

Our analysis has been concerned in proving the superiority of the readings from the on-board accelerometer with respect to the modelling of the non-conservative

accelerations due to the NGP. Indeed, the analysis presented in this paper modelled the long-period NGP in length in its first and major part. In its second part, the short-period NGP only have been considered in their relation to the accelerometer features.

This means that—during the MPO orbit determination—the accelerometer readings are just added to the equations of motion containing the gravitational terms only. In particular, the orbit propagation error is driven by the accelerometer measurement error. This acceleration error is related to the accelerometer sensitivity, if integrated over the observational time span necessary for the MPO orbit fit. It is typically two-orders-of-magnitude smaller than the acceleration due to the direct solar radiation pressure.

The main results achieved with this work can be summarised as follows:

1. we have estimated the long-period behaviours of the three components in the Gauss co-moving frame of the disturbing NGP acceleration due to: (i) direct solar radiation pressure and (ii) Mercury's albedo radiation pressure. The maximum amplitudes and spectral contents have been derived;
2. these amplitudes and frequencies are important in order to correctly establish which are the main components of the disturbing accelerations (and therefore the main disturbed sensitive axes of the accelerometer), and which are the main long-period thermal disturbing effects on the MPO and, finally, on the accelerometer;
3. the largest orbit perturbations are due to SRP, accelerations vary in the range $4 \cdot 10^{-7}$ m/s$^2 \div 1 \cdot 10^{-6}$ m/s^2, because of the large eccentricity of Mercury's orbit and the very large variations of the solar irradiance over Mercury's sidereal period;
4. in the case of the solar radiation the largest effects on the accelerometer axes are produced by the out-of-plane component of the acceleration (with a maximum amplitude of about $8 \cdot 10^{-7}$ m/s^2 and a very strong spectral line ($\dot{\lambda}$, with $S^{1/2} \simeq 0.95$) at the sidereal period of Mercury (about 88 days)), and by the radial component of the acceleration (with a maximum amplitude of about $2.5 \cdot 10^{-7}$ m/s^2 and a stronger spectral line ($2\dot{\lambda}$, with $S^{1/2} \simeq 0.75$) at half of the sideral period of Mercury (about 44 days));
5. therefore, the prominent thermal effects are at the sidereal period of Mercury (88 days) and at half of the sidereal period of Mercury (44 days), in agreement with previous analyses conducted by ESA industrial contractors;
6. the transversal component of the disturbing acceleration is responsible for thermal effects with frequencies $\dot{\omega} \pm \dot{\lambda}$. Their corresponding periodicities are very close to the sidereal period of Mercury—86.05 days and 89.99 days—and their intensities ($S^{1/2} \simeq 0.35$) are smaller than those produced by the radial or out-of-plane components;
7. the long-period peak amplitudes of the transversal acceleration are about a factor 10 smaller than those of the radial component of the solar acceleration, i.e., the accelerometer sensitive axis along the transversal direction is less influenced by the solar radiation. This is particularly important for the rôle played by the transversal acceleration in the RSE and because it is less influenced by the accelerometer calibration than the radial and out-of-plane components. Anyway, the simulations that have been performed in the past considered only a thermal signal with a 44-days period for each axis of the accelerometer. In the light of the present results it will be useful if these simulations will be repeated considering,

for each component of the disturbing acceleration, the correct thermal effect with its own amplitude and period: 44 days for the radial component, 88 days for the out-of-plane component, and two signal with periods of about 90 days and 86 days for the transversal component;

8. however, as we have seen, the impact of the thermal signals on the accelerometer is controlled by the accelerometer intrinsic stability to temperature variations (presently equal to $5 \cdot 10^{-7}$ m/s^2/°C) and an active thermal control, as described in Sect. 2.2, will be used, see also Iafolla et al. 2006);
9. the impact on the MPO orbit of the solar radiation pressure has been estimated through the use of the Gauss perturbing equations. The corresponding variations on the MPO orbital elements $(a, e, I, \Omega, \omega)$ have been derived. The impact on the orbital elements is dramatic, their changes are more than two-orders-of-magnitude larger than those of the Earth-orbiting LAGEOS II satellite. Moreover, the solar radiation perturbation is even larger than the gravitational perturbations produced by the main zonal harmonic coefficients of Mercury's gravity field, as we have verified in the case of the MPO eccentricity and argument of perigee for the first even zonal harmonic coefficient C_{20};
10. also in the case of the albedo radiation we have found large effects on the MPO orbit. However, the magnitude of the three components of the disturbing acceleration is smaller than the values obtained in the case of the solar radiation, especially for the transversal component. The impact on the orbital elements has been estimated to be about two orders-of-magnitude smaller in the rates of the analysed elements than in the case of the solar radiation;
11. the MPO orbit analysis during the RSE for the gravity field recovery and general relativity testing, is performed over short arcs of a few hours length. It is therefore of fundamental importance to understand, how much we are able to gain over this arc length with the use of an accelerometer instead of modelling the NGP effects. This kind of analysis has been conducted over a time span equal to three orbital revolutions of the MPO spacecraft around Mercury (about 7 h).

    We have shown that the SRP acceleration is measured, and aposteriori removed, with a 1% accuracy (i.e., its impact on the MPO orbit determination is reduced by a factor of 100) with the use of an on-board accelerometer. This result is valid if no modelling is assumed for this disturbing acceleration and an accelerometer measurement error of about 10^{-8} m/s^2—equal to the accuracy necessary to reach the ambitious goals of the RSE—is assumed over the entire bandwidth of the ISA accelerometer (see Figs. 17 and 18), or at least in the 10^{-4}–10^{-3} Hz interval;
12. however, a few points need to be considered: (i) the accelerometer performances should be compared to the best modelling we can reach for the NGP, in particular in view of the strong solar radiation pressure, rather than to the no-modelling results, (ii) even assuming best modelling efforts, we are not able to model correctly the satellite transition in and out of the eclipses during the penumbra passages (on the contrary such effects will be recorded by the accelerometer), (iii) the ISA accelerometer accuracy noise is about 10^{-8} m/s$^2/\sqrt{\text{Hz}}$ in the frequency band $3 \cdot 10^{-5}$–10^{-1} Hz.

    Therefore, while item (i) reduces the gain that we have with the use of the accelerometer to a factor of 10 only (because we are not able to model the NGP with an accuracy better than 10%, as explained in Sect. 5.1), items (ii) and (iii) increase the gain. Of course, the increase of accuracy from item (iii) depends on

integration time span and on the possibility to constrain all the other sources of noise to an appropriate accuracy level, as explained in Sect. 5.1.

The ESA BepiColombo mission to Mercury is planned to be launched in 2013 and will reach Mercury in 2019. However, BepiColombo will not be the first mission to Mercury after the three flybys of NASA's Mariner 10 spacecraft (1974–1975). The NASA MESSENGER (MErcury, Surface, Space ENvironment, GEochemistry, and Ranging) mission will indeed send the first spacecraft to orbit Mercury. On August 3, 2004, MESSENGER has been launched successfully from Cape Canaveral and will reach Mercury in 2009. The main goals of MESSENGER are identical to those of BepiColombo: the geological evolution of the planet, its internal structure composition, its surface chemical composition and the origin of Mercury's magnetic field (Solomon et al. 2001; Gold et al. 2001). The general relativity tests will not be specific objectives of the MESSENGER mission, altough some improvements could be achieved with respect to the present knowledge of the post-Newtonian parameters. Anyway, no accelerometer is flying on the NASA spacecraft and this will seriously limit the final accuracy of the MESSENGER experiments if compared to those of BepiColombo.

Of course, BepiColombo will benefit from the MESSENGER mission to Mercury under several aspects. Some of the these advantages are linked to the studies of the non-gravitational forces and their impact on the Mercury orbiter. For instance, with MESSENGER we will reach an almost complete description of all the planet surface and albedo features. This will allow us to build up a grid of the albedo distribution and, therefore, in principle, we will be able to model in a more refined way (if necessary) the albedo perturbation on the complex shape of the MPO satellite. Also the infrared emissivity of the planet will be better resolved.

In a forthcoming paper, the present work will be extended to the NGP due to Mercury's infrared radiation. The infrared radiation effects are much smaller in amplitude than those produced by the solar radiation pressure, the order-of-magnitude of the perturbation is close to the albedo radiation effects. Anyway, because of the huge latitudinal excursion of temperature across Mercury's surface, and the strong day/night asymmetry, it is useful to estimate their impact on the MPO orbit as well as their contribution to the disturbing thermal effects. Another interesting perturbation to be analysed in the future is that produced by the spacecraft thermal emission. Finally, ISA error budget and its inflight calibration procedures will be the subjects of other two dedicated papers.

Acknowledgements The authors are grateful to A. Milani (Pisa University, Italy), A. Rossi (ISTI/CNR, Italy) and to L. Iess (Roma University, Italy) for providing input for this research. Special thanks to two anonymous reviewers for helpful comments and suggestions. D. L. is also grateful to the staff of the SpaceFlight Dynamics Laboratory for kind hospitality at ISTI/CNR during these years.

References

Anderson, J.D., Colombo, G., Esposito, P.B., Lau, E.L., Trager, G.B.: The mass, gravity field and ephemeris of Mercury. Icarus **71**, 337–349 (1987)

Baker, R.M.L.: Astrodynamics, p. 193. Academic Press, New York and London (1967)

Barlier, F., Carpino, M., Farinella, P., Mignard, F., Milani, A., Nobili, A.M.: Nongravitational perturbations on the semimajor axis of LAGEOS. Ann. Geophys. **4A**, 193–210 (1986)

Bertotti, B., Iess, L., Tortora, P.: A test of general relativity using radio links with the Cassini spacecraft. Lett. Nat. **425**, 374–376 (2003a)

Bertotti, B., Farinella, P., Vokrouhlicky, D.: Physics of the Solar System, Chapter 14. Kluwer Academic Publishers (2003b)
Cohen, S.C., Smith, D.E.: LAGEOS scientific results: Introduction. J. Geophys. Res. **90**(B11), 9217–9220 (1985)
Ferraz–Mello, S.: Analytical study of the Earth's shadowing effects on satellite orbits. Celest. Mech. **5**, 80–101 (1971)
Gold, R.E., Solomon, S.C., McNutt, R.L., et al.: The MESSENGER mission to Mercury: scientific paylod. Plan. Space Sci. **49**, 1467–1479 (2001)
Grard, R., Balogh, A.: Returns to Mercury: science and mission objectives. Plan. Space Sci. **49**, 1395–1407 (2001)
Iafolla, V., Nozzoli, S.: Italian spring accelerometer (ISA) a high sensitive accelerometer for "BepiColombo" ESA CORNERSTONE. Plan. Space Sci. **49**, 1609–1617 (2001)
Iafolla, V., Lucchesi, D.M., Fiorenza, E., Nozzoli, S.: On the ISA Accelerometer Positioning inside the Mercury Planetary Orbiter. To be published by Plan. Space Sci. (2006)
Iess, L., Boscagli, G.: Advanced radio science instrumentation for the mission BepiColombo to Mercury. Plan. Space Sci. **49**, 1597–1608 (2001)
Kozai, Y.: The motion of a close Earth satellite. The Astron. Journ. 367–377 (1959)
Lucchesi D.M., Farinella, P.: Optical properties of the Earth's surface and long-term perturbations of LAGEOS's semimajor axis. J. Geophys. Res. **97**(B5), 7121–7128 (1992)
Lucchesi, D.M.: Reassessment of the error modelling of non-gravitational perturbations on LAGEOS II and their impact in the lense-thirring determination. Part I. Plan. Space Sci. **49**, 447–463
Lucchesi, D.M., Balmino, G.: The LAGEOS satellites orbital residuals determination and the Lense-Thirring effect measurement. Plan. and Space Sci. **54**, 581–593 (2006)
Milani, A., Nobili, A.M., Farinella, P.: Non-Gravitational Perturbations and Satellite Geodesy. Adam Hilger, Bristol (1987)
Milani, A, Carpino, M., Rossi, A., Catastini, G., Usai, S.: Local Geodesy by satellite laser ranging: an European solution. Manuscripta Geodetica **20**, 123–138 (1995)
Milani, A., Rossi, A., Vokrouhlick, D., Villani, D., Bonanno, C.: Gravity field and rotation state of Mercury from the BepiColombo Radio Science Experiments. Plan. Space Sci. **49**, 1579–1596 (2001)
Milani, A, Vokrouhlicky, D., Villani, D., Bonanno, C., Rossi, A.: Testing general relativity with the Bepicolombo radio science experiment. Phys. Rev. D **66**, 082001 (2002)
Rubincam, D.P., Weiss, N.R.: Earth albedo and the orbit of LAGEOS. Celest. Mech. **38**, 233–296 (1986)
Solomon, S.C., McNutt, R.L., Gold, R.E., et al.: The MESSENGER mission to Mercury: scientific objectives and implementation. Plan. Space Sci. **49**, 1445–1465 (2001)
Smith, R.E., West, G.S., compilers: Space and planetary environment criteria guidelines for use in space vehicle development, 1982 revision. NASA TM–82478 (1983)
Spohn, T., Sohl, F., Wieczerkowski, K., Conzelmann V. The interior structure of Mercury: what we know, what we expect from BepiColombo. Plan. Space Sci. **49**, 1561–1570 (2001)
Tapley, B.D., Schutz, B.E., Born, G.H.: Statistical Orbit Determination. Elsevier, Academic Press (2004)
Vilas, F., Chapman, C.R., Matthews, M.S.: Mercury. The University of Arizona Press, Tucson (1988)
Vokrouhlický, D., Farinella, P., Mignard, F.: Solar radiation pressure perturbations for Earth satellites. I: A complete theory including penumbra transitions. Astron. Astrophys. **280**, 295–312 (1993)
SCI–PB/RS/1140. Experiment Interface Document. Part A. ESA.